Eur. Phys. J. D **58**, 181–186 (2010)
DOI: 10.1140/epjd/e2010-00061-4

THE EUROPEAN PHYSICAL JOURNAL D

Regular Article

Labyrinth bifurcations in optically injected diode lasers

V. Kovanis[1], A. Gavrielides[2], and J.A.C. Gallas[3,4,5,a]

[1] Air Force Research Laboratory, 2241 Avionics Circle, Wright-Patterson AFB, Dayton OH 45433, USA
[2] USAF, Research Laboratory, High Power Solid State Lasers Branch, Kirtland AFB, NM 87117, USA
[3] TecEdge, Wright Brothers Institute, 5100 Springfield Street, Dayton OH 45431, USA
[4] Departamento de Física, Universidade Federal da Paraíba, 58051-970 João Pessoa, Brazil
[5] Instituto de Física, Universidade Federal do Rio Grande do Sul, 91501-970 Porto Alegre, Brazil

Received 29 December 2009
Published online 16 March 2010 –

Abstract. Although pulsating and chaotic regimes in injection-locked semiconductor lasers have been described often in the literature, so far their relative abundance has remained poorly explored. Here, for two popular laser models, we report detailed Lyapunov phase (stability) diagrams characterizing the extension in parameter space of pulsating phases. Our phase (stability) diagrams discriminate regular from chaotic laser emissions and indicate where multistability is to be expected in injection-locked semiconductor lasers.

1 Introduction

It has long been recognized that the free-running relaxation oscillation of a semiconductor laser is the key physical element that needs to be judiciously modified to obtain high-speed semiconductor laser devices which may then be incorporated in a myriad of photonic applications in commercial as well as in defense settings. Typically, speeds are limited to a few GHz. During the past few years, however, many photonic approaches have been introduced, debated, and experimentally implemented as well as theoretically investigated. Such techniques are based on strong optical injection of diode lasers, introducing optical coupling between two or more gain sections, and externally feeding light back into the lasing cavity.

An interesting development concerning the dynamical behaviour of optically injected semiconductor lasers is the experimental observation of period three (P3) oscillations close to a period doubling bifurcation of the fundamental limit-cycle of the laser [1]. The P3 regimes were identified experimentally and it was found that they lie in a small regime of detuning around zero. Calculations using a full model based on a rate equations agreed very well with the experimental observations. Additionally, a simplified asymptotic model was introduced that captures the essential features of the P3 bifurcation. Using a continuation tool, the bifurcation features for several values of the damping were computed and it was demonstrated that the limit-point of the P3 bifurcation lies very close to the first period-doubling of the P1 solution. Additionally, the branch of stable P3 solutions undergoes several period-doubling bifurcations.

Independent experiments on period-three oscillations were also reported by Eriksson and Lindberg [2,3] who measured the location and magnitude of period-three cycles characterized by regular oscillations existing inside chaotic phases of semiconductor lasers. By working on a two-parameter control space (codimension two), they identified a period-three cycle by tuning the injection intensity for three fixed values of the frequency detuning. Then, by repeating measurements for finer detuning intervals, they characterized a few limit-cycles of low period. With much higher resolution, such two-parameter laser stability diagrams were recently corroborated and greatly extended by numerical simulations which uncovered a myriad of additional periodic cycles of ever-increasing periods, forming regular parameter networks, and accumulating in rather systematic and novel ways [4,5]. The distinction between the experimental work of [1] and the experiments of [2,3] is that the limit-cycles in the latter appear in the chaotic regime, following a scenario that has been found previously in several systems including the quadratic map. In contrast, in reference [1] the P3 bifurcations emerge from saddle-node bifurcations. Numerical computations using continuation methods have found P3 isolas for large negative detunings [6–8], but isolas have not been reported for zero or very small detunings as in the experiments and computations of reference [1].

As may be seen in Figure 1, the two-parameter control space of the injection-locked semiconductor laser presents a very intricate structure with a number of features remaining unclear and that will be explored here. More precisely, the purpose of this paper is to delimit numerically the extension of periodic and chaotic oscillations supported by two laser models. This is done by investigating the dynamics under the simultaneous variation of

[a] e-mail: jgallas@if.ufrgs.br

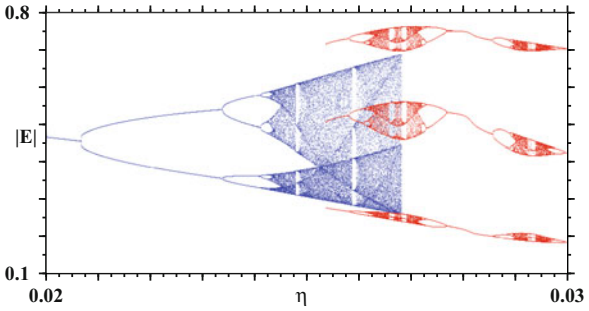

Fig. 1. (Color online) Coexistence of pulsating laser modes, indicated by the overlap of the blue and the red bifurcation diagrams of the minima of $|E|$, computed according to the *full* laser model of equations (1)–(2). The red period-3 modes display "period bubbling" [12].

two handy control parameters of the laser, namely the injection strength and the laser detuning. We find that experimentally observed oscillations form self-similar islands of stability embedded in chaotic phases. In particular, the period-three oscillations are found to be the first of an infinite cascade of limit-cycles embedded in the chaotic regime and extending well into the region of positive detunings.

Landmark manuscripts in injection are the 1948 Adler paper on injection where the celebrated equation is formulated [9], the Bell labs manuscript on injection in CO_2 lasers, and the work of Lang [10] that introduced the role of the phase amplitude coupling (i.e. linewidth enhancement factor) in the dynamics of optically injected lasers. His findings are summarized as follows: the injection locking properties of a semiconductor laser have been analyzed taking into account the injected carrier density dependent refractive index in the active region. It has been found that this dependence significantly affects the injection locking properties, giving rise to a peculiar asymmetric tuning curve and dynamic instability. The instability originates from the intermode interaction via the modulation in the injected carrier density caused by intensity beat. The detuning dependence of the direct modulation response characteristics inside and outside of the locking range have also been examined, in a key manuscript of 1995 [11] that finished the job that Lang started, by introducing two new ingredients in the dynamical behaviour of optical injection, namely, the fast frequency issue and the restabilization of the slave via a reverse Hopf bifurcation in the strong injection region.

In this paper we review stability issues associated with optically injected semiconductor lasers as one varies the optical frequency detuning and the injection level but keeping other key parameters fixed: linewidth enhancement factor, nonlinear gain coefficient and above-threshold pumping level. The manuscript is organized as follows: in section two a pair of simple model rate equations are introduced and all the physical parameters are named, the rescaling to more "natural" physical parameters is in turn introduced and the models are written in such forms that they connect with legacy theoretical work and in forms that facilitate the numerical computation. In this way, legacy work (theoretical and experimental) on the stability problem of optically injected semiconductor lasers is put in context. In section three the stability work is presented in a series of numerical computations, the computation method is detailed, and all findings are explained and discussed in the context of bifurcation theory. Finally, in the last section conclusions are drawn and implications are inferred for future work. In addition, some implications for new kinds of lasers are forecast.

2 The full and the simplified laser models

Following Gavrielides et al. [1], in this section we review briefly two popular laser models, called "full" and "simplified" as in the original work. In dimensionless form, the full model is defined by two non-autonomous equations for the complex electric field $E \equiv E_x + iE_y$ and the excess carrier number N, namely,

$$\dot{E} = (1 - ib)GE + \eta \exp(-i\Omega t), \tag{1}$$

$$T\dot{N} = P - N - P(1 + 2G)|E|^2. \tag{2}$$

These equations are equivalent to a four-dimensional autonomous system. In the equations above, the time is measured in units of the photon lifetime τ_p and the nonlinear *gain* $G = G(N, E)$ is defined by

$$G \equiv N - \varepsilon P\left(|E|^2 - 1\right), \tag{3}$$

taking into account the effect of gain saturation if $\varepsilon \neq 0$.

The rightmost term in equation (1) models the injected signal, which is characterized by its amplitude η and the optical frequency detuning Ω, the difference between the master and slave laser optical frequencies. The linewidth enhancement factor is denoted by b and lies typically in the interval $3 \leq b \leq 6$. It quantifies the degree of amplitude phase coupling. The parameter $T \equiv \tau/\tau_p$ is the ratio of the carrier to photon lifetimes, while P is the dimensionless pumping current above threshold.

While searching for period-three laser oscillations, Gavrielides et al. [1] considered also a *simplified* form of the full laser model defined by equations (1) and (2). These equations were derived in the asymptotic limit of large b, a limit which had earlier been found convenient for analyzing period-doubling bifurcations [13]. Specifically, they neglected the effect of gain saturation by setting $\varepsilon = 0$ and introduced new variables a, Φ, n and s defined by

$$E \equiv \left(1 + \frac{a}{b}\right) e^{i\Phi}, \qquad n \equiv \frac{\omega N}{b}, \qquad s \equiv \omega t, \tag{4}$$

where $\omega \equiv \sqrt{2P/T}$ is the normalized laser relaxation oscillation frequency. Inserting the new variables above into equations (1) and (2) with $\varepsilon = 0$ in equation (3) and taking the limit $b \to \infty$ while retaining the leading order in $1/b$ leads to the following simplified autonomous three-dimensional model:

$$\dot{a} = n + \Lambda \cos\Phi, \tag{5}$$

$$\dot{\Phi} = \Delta - n, \tag{6}$$

$$\dot{n} = -\xi n - a, \tag{7}$$

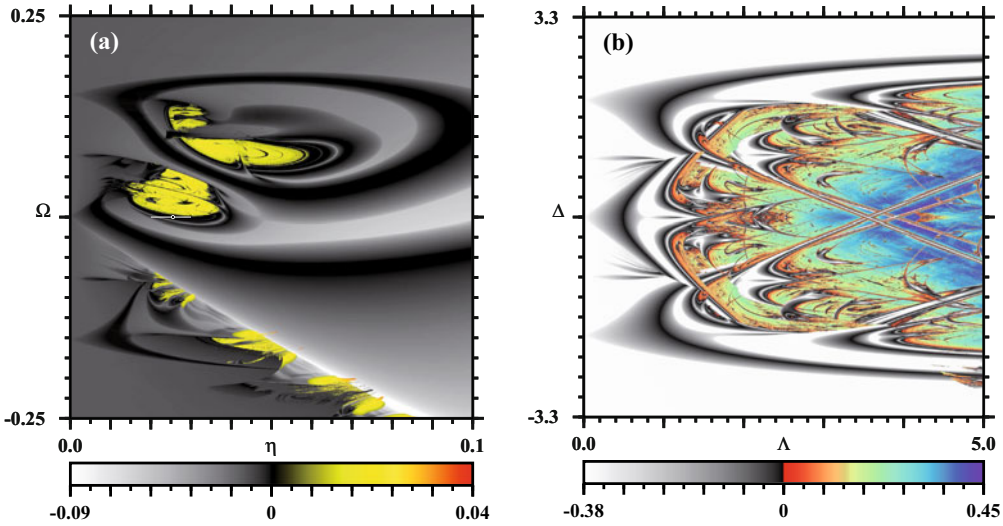

Fig. 2. (Color online) Comparison of Lyapunov phase diagrams computed with the *full* laser model (left panel) and with the *simplified* model (right). Each diagram displays 2000^2 Lyapunov exponents. Parameters for the full model: $b = 3.2$, $\varepsilon = 0.011$, $P = 0.48$, $T = 165$; in the simplified model $\xi = 0.5$. The small horizontal white line segment along $\Omega = 0$ marks the period-three isola considered in the bifurcation diagram in Figure 4 of Gavrielides et al. [1]. The black dot along the line marks parameters used to generated the basins of attraction shown in Figure 5.

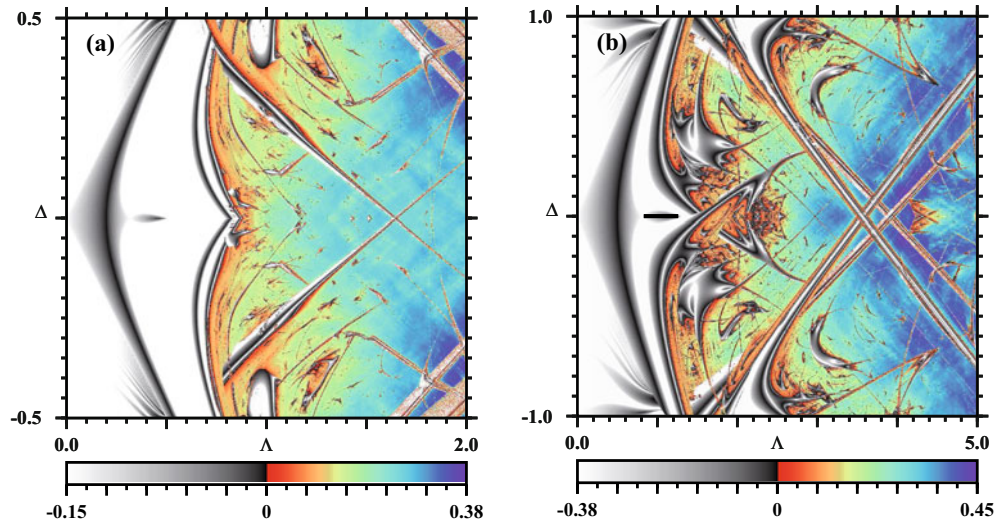

Fig. 3. (Color online) Phase diagrams computed with the *simplified* laser model of equations (5)–(7). Left: $\xi = 0.2$; right: $\xi = 0.5$. The black line segment along $\Delta = 0$ in the right panel indicates the interval $0.83 \leq \Lambda \leq 1.26$ of Figure 3 of reference [1], at the end of which period three was found. Note the abundance of intersections, where multistability exists. The rightmost panel shows a magnification of part of Figure 2b.

where $\xi \equiv (1 + 2P)\omega/(2P)$ is known as the linear damping rate of the laser relaxation oscillations, and in which the derivatives are now taken with respect to s. The new control parameters Λ and Δ in equations (5)–(7) are proportional to η and Ω, respectively, and are defined by

$$\Lambda \equiv \frac{\eta b}{\omega} \qquad \text{and} \qquad \Delta \equiv \frac{\Omega}{\omega}. \tag{8}$$

By eliminating a and n, equations (5)–(7) may be written as a single third-order differential equation for Φ, namely,

$$\dddot{\Phi} + \xi\ddot{\Phi} + \dot{\Phi} = \Delta + \Lambda\cos\Phi. \tag{9}$$

As pointed out by Gavrielides et al. [1], the main advantage of equation (9) is the fact that it depends on only three control parameters: ξ, Λ and Δ. Analytical approximations for the solutions of equations (5)–(7) have been derived in references [14,15].

For $T = 165$, $b = 3.2$, $P = 0.48$, $\Omega = 0$, $\varepsilon = 0.011$ one finds $\omega = \sqrt{2P/T} = 0.076277$ and that the injection interval $0.02 \leq \eta \leq 0.03$ used in Figure 2 corresponds to the Λ-interval

$$0.83 \leq \Lambda \leq 1.26. \tag{10}$$

This interval is shown by a black line segment in Figure 3. Period three was first observed at the end of this line segment [1].

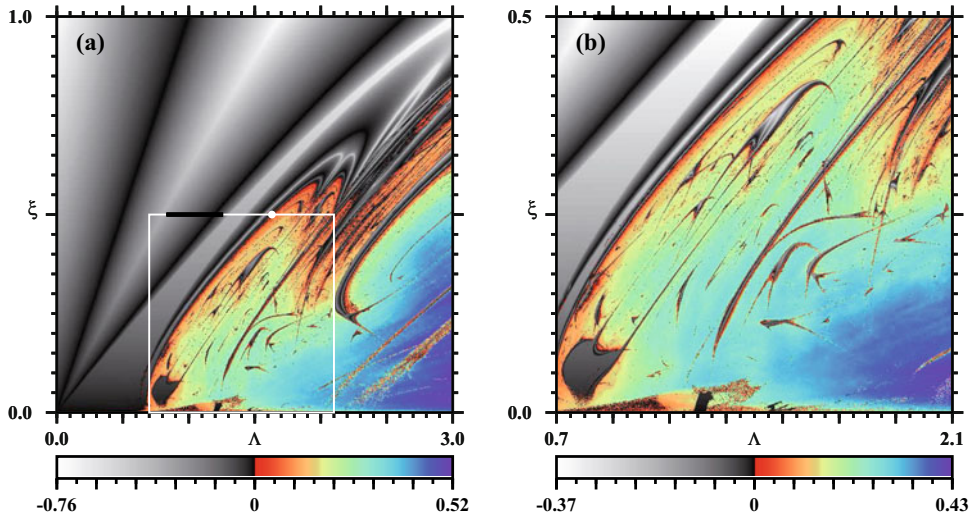

Fig. 4. (Color online) Phase diagrams computed with the *simplified* laser model with $\Delta = 0$. The white box is magnified in the right panel. The dark line segment along $\xi = 0.5$ in the white box marks the interval $0.83 \leq \Lambda \leq 1.26$ considered in Figure 3 of reference [1], at the end of which period three was found. A wide chaotic region exists on the right side of $\Lambda \gtrsim 1.63$, the value indicated by the white dot. Each panel displays 1200^2 Lyapunov exponents.

3 Bifurcation and phase diagrams

Using the full and simplified laser models defined in the previous section, we computed the pair of bifurcation diagrams shown in Figure 1 and a number of two-parameter Lyapunov phase diagrams characterizing the dynamical behaviours (stability regions). As is known, Lyapunov exponents are practical indicators that allow one to discriminate regular from chaotic *stable* laser oscillations. Positive exponents indicate chaotic solutions while negative exponents denote regular laser oscillations. Examples of Lyapunov phase-diagrams are shown in Figures 2–4. The scales under each phase diagram indicate the convention used here to discriminate chaos from periodicity: colours are used to represent chaotic oscillations (i.e. positive Lyapunov exponents) while regular oscillations are shown using darker tonalities (negative exponents).

Our phase diagrams were obtained by computing the full spectra of Lyapunov exponents for selected regions of the parameter space over a very fine mesh of $L \times L$ equally spaced points, $L = 1200$ and $L = 2000$ being typical values. Normally, phase diagrams where computed horizontally from left to right starting always from an arbitrary but fixed initial condition on the left border and proceeding by "following the attractor", namely by using the last obtained values of the variables to start new integrations after having incremented parameters infinitesimally. For further details see references [16–23] and references therein.

The "bridge" provided by the pair of relations defined in equation (8) allows one to compare parameter windows computed with the full and the simplified laser models. Such a comparison is presented in Figure 2, where the exact relation between parameter intervals is as follows:

$$0 \leq \eta \leq 0.1 \quad \Longleftrightarrow \quad 0 \leq \Lambda \leq 4.2, \tag{11}$$

$$-0.25 \leq \Omega \leq 0.25 \quad \Longleftrightarrow \quad -3.3 \leq \Delta \leq 3.3. \tag{12}$$

Figure 2a shows a relatively wide portion of the parameter space centered around a particular line of parameters, indicated by the white segment along $\Omega = 0$. Figure 2b shows the corresponding window as generated with the simplified model. The white parameter line in Figure 2a is interesting because it contains parameters leading to period-three oscillations [1]. As already mentioned, dark regions correspond to parameters leading to regular laser output while colours denote regions supporting chaotic laser modes. The evolution of the laser modes along the white segment is shown in detail in the pair of bifurcation diagrams in Figure 1. In addition to period three, the overlap of the two bifurcation sequences in Figure 1 shows unambiguously the existence of multistability in the system. Multistability persists over wide portions of parameter space. The phase diagram in Figure 2a is similar to diagrams reported in references [4,5], despite the fact that they were obtained for a distinct laser model and distinct parameters.

Comparing Figures 2a and 2b, i.e. comparing the phase diagrams obtained for the full and simplified laser models, it is easy to see that both models agree quite well up to about $\Lambda \simeq 0.5$ (i.e. up to $\eta \simeq 0.012$). The agreement is good both for positive and for negative detuning. It is also clear that both models predict the abundance of rather complicated chaotic phases and that the structure of such phases depends on the model considered. This dependence is not surprising since the simplified model was derived to assist in obtaining analytical results only up to moderately strong amplitudes η of the injected signal. Note the symmetry of Figure 2b with respect to the axis $\Delta = 0$, a consequence of the invariance of equations (5)−(7) (or, equivalently, of equation (9)) with respect to any of the substitutions

$$(\Phi, \Delta) \longrightarrow (-\Phi \pm \pi, -\Delta). \tag{13}$$

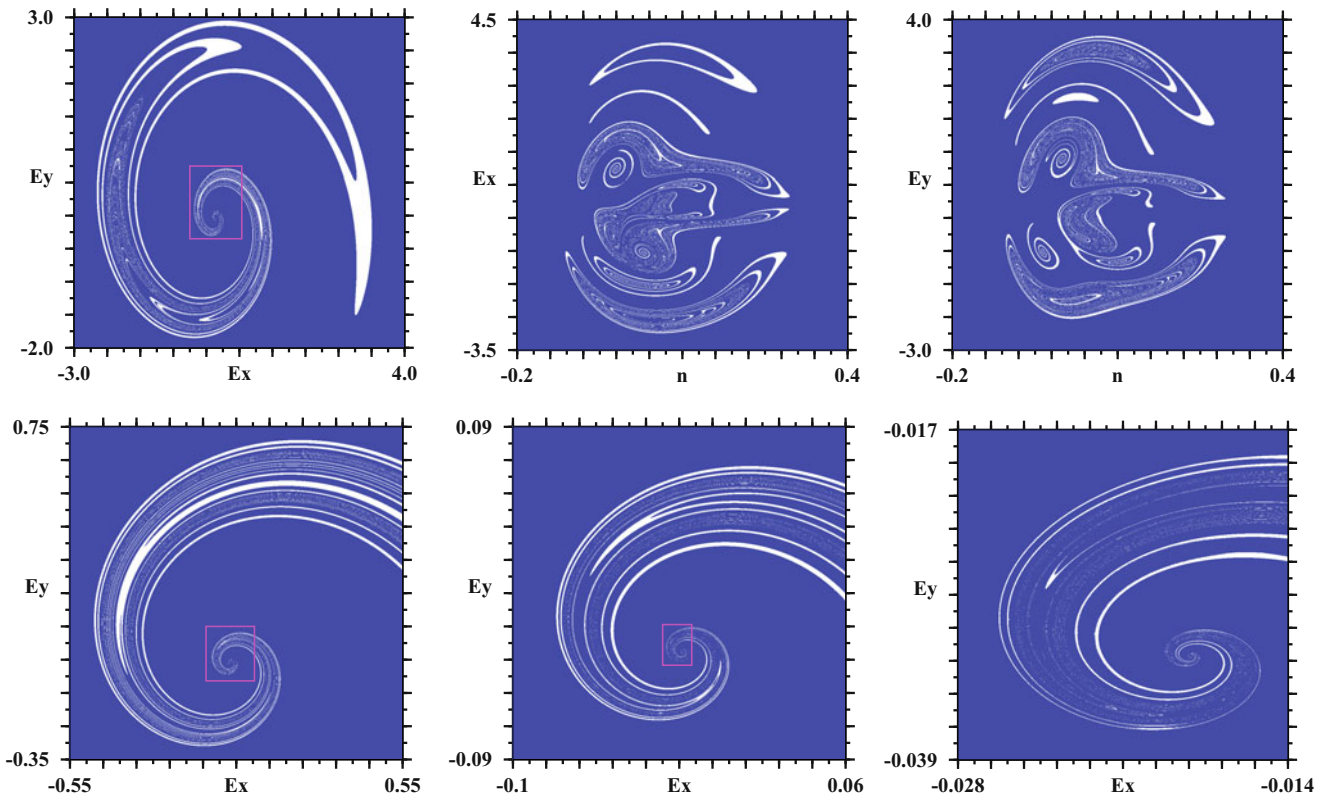

Fig. 5. (Color online) Basins of attraction computed with the *full* model. Top row: projections on the planes $(E_x, E_y, 0)$, $(E_x, 0, n)$, and $(0, E_y, n)$. Note the several spirals present in the phase space. Bottom row: successive magnifications of the box in the leftmost panel of the top row showing the self-similarity ("fractality") of the basins. Here $\eta = 0.0255$, $b = 3.2$, $\varepsilon = 0.011$, $P = 0.48$, $T = 165$, $\Omega = 0$. Each panel displays 800^2 Lyapunov exponents.

Note also the abundance of multistability and that the simplified model allows coexistence of several symmetrical modes. We will not attempt to describe here the structure of multistable laser modes, the chaotic phases and the plethora of periodic windows embedded in them. They form a vast and intricate labyrinth of proliferating bifurcation possibilities in which it is easy to lose the way, in the same manner as nicely described by Borges in a rather different context [24].

The simplified model of equations (5)–(7) involves a three-parameter control space, Λ, Δ, ξ, and Figures 3 and 4 illustrate two additional sections of this parameter space. Figure 3 shows the $\Delta = 0$ parameter section for $\xi = 0.2$ (left panel) and $\xi = 0.5$ (right panel). These figures illustrate the rich dynamics that exists near $\Delta = 0$, the value for which the bifurcation diagram containing period-three in Figure 1 was computed. In Figure 3b we indicate with a black line segment the location of the interval $0.83 \leq \Lambda \leq 1.26$ along $\xi = 0.5$, the period-three interval discussed at length in reference [1]. Figures 3 and 4 contain wide portions in colour, indicating abundance of chaotic oscillations. Such chaotic phases contain complicated distributions of dark phases representing periodic laser modes. As is easy to recognize from Figure 3a, for $\xi = 0.5$ a wide chaotic domain is located at higher values of Λ, starting near $\Lambda = 1.63$ – the value indicated by the white dot. The diagram for $\xi = 0.5$ is shifted to the right and the Hopf bifurcation appears at a large value of Λ as predicted from a simple analysis that shows that for the Hopf bifurcation Λ is about equal to ξ. In Figures 3 and 4 it is easy to recognize a plethora of regions where domains of distinct periodicities overlap, indicating coexistence of periodic laser oscillations. In this context, a natural problem is to locate domains where *chaotic* phases overlap, i.e. domains where more than one chaotic laser oscillation would be possible.

Figure 4 illustrates portions of the $\Lambda \times \xi$ space for $\Delta = 0$. As is clear from Figure 4a, chaos prevails in almost 50% of the parameter region considered, which is quite large. The distribution of domains of regularity embedded in the chaotic phase show a structure that is even more complex than that predicted for the parameter section shown in Figure 3, displaying no obvious organization.

As our last result, Figure 5 presents basins of attraction obtained for the full laser model computed for the parameter point indicated in Figure 2a. In other words, Figure 5 presents two-dimensional cuts of phase-space of the full laser model. To obtain this figure, we first computed histograms of the Lyapunov exponents and counted the distinct peaks in the diagram, attributing a colour to each peak. The blue colour represents the basin of attraction of a chaotic attractor having its maximum positive Lyapunov centered near $\lambda_1 \simeq 0.006$. In this particular point of parameter space, the chaotic attractor coexists

with a period-three attractor, whose basin is represented here in white. As the several magnifications in the bottom row show, the phase space has a fractal-like structure here. This type of basin structure was found to be quite common in this region of the parameter space.

4 Conclusions and outlook

To summarize, we have presented detailed Lyapunov phase diagrams characterizing the regions of stable operation of two popular models which are known to reproduce well experimental results of injection-locked semiconductor lasers. Our phase diagrams show the distribution of periodic and chaotic laser modes across wide ranges of injection intensities and for both positive and negative detuning. Of particular interest is the region of moderate and large negative detunings where the coexistence of steady and pulsating intensities is quite unusual since they correspond to separate branches not connected by Hopf bifurcation points [1]. Our diagrams complement earlier results by describing how steady states and periodic modes are organized in parameter space, how they are interconnected, and their relative abundance, answering questions that have remained so far not explored due to the heavy computational workload required to answer them. Our phase diagrams indicate also where multistability is to be expected in injection-locked semiconductor lasers. We re-iterate: our diagrams display only *stable* solutions, i.e. stable phases, those that are more easily accessible in experiments.

An enticing open problem now is to characterize the full extension and shape of the boundaries of regions where labyrinth bifurcations and chaos occur, namely where *coexistence* of chaotic oscillations is to be expected. Such regions with labyrinthian bifurcations that display coexistence of chaotic signals and periodic limit-cycles are of great interest in chaos-based secure communications [25]. With chaos-enabled random number generators it is expected that the performance of random number generators can be greatly improved by using chaotic laser devices as physical entropy sources [26,27]. And, finally, labyrinthian bifurcations are also expected to have an impact in a whole host of next generation RF photonics subsystems such as remote sensors of laser radiation [28], chaotic RADAR [29], laser radar and optical systems that generate passively diverse arbitrary waveforms [30,31] where, for example, preliminary experiments based on an optically injected geometry show subcentimeter accuracy in ranging with a 3-cm-range resolution.

JACG thanks support from the Air Force Office of Scientific Research, Grant FA9550-07-1-0102, and CNPq, Brazil. All computations were done in the Sun Fire X2200 and X4600 clusters of the CESUP-UFRGS, in Porto Alegre. VK thanks support from AFOSR.

References

1. A. Gavrielides, V. Kovanis, M. Nizette, T. Erneux, T. Simpson, J. Opt. B: Quantum Semiclass. Opt. **4**, 20 (2002)
2. S. Eriksson, A. Lindberg, Opt. Lett. **26**, 142 (2001)
3. S. Eriksson, A.M. Lindberg, J. Opt. B: Quantum Semiclass. Opt. **4**, 149 (2002)
4. C. Bonatto, J.A.C. Gallas, Phys. Rev. E **75**, 055204(R) (2007)
5. C. Bonatto, J.A.C. Gallas, Phil. Trans. R. Soc. Lond. A **366**, 505 (2008)
6. S. Wieczorek, B. Krauskopf, D. Lenstra, Opt. Commun. **183**, 215 (2000)
7. S. Wieczorek, B. Krauskopf, D. Lenstra, Phys. Rev. E **64**, 056204 (2001)
8. S. Wieczorek, B. Krauskopf, T.B. Simpson, D. Lenstra, Phys. Rep. **416**, 1 (2005)
9. R. Adler, Proc. IRE **34**, 351 (1946); reprinted in Proc. IEEE **61**, 1380 (1973)
10. R. Lang, IEEE J. Quantum Electron. **18**, 976 (1982)
11. T.B. Simpson, J.M. Liu, A. Gavrielides, V. Kovanis, P.M. Alsing, Phys. Rev. A **51**, 4181 (1995)
12. M. Bier, T.C. Bountis, Phys. Lett. A **104**, 239 (1984)
13. T. Erneux, V. Kovanis, A. Gavrielides, P.M. Alsing, Phys. Rev. A **53**, 4372 (1996)
14. A. Gavrielides, V. Kovanis, P.M. Varangis, T. Erneux, G. Lythe, Quantum Semiclass. Opt. **9**, 785 (1997)
15. D. Sukow, V. Kovanis, A. Gavrielides, VII Proc. SPIE **3625**, 778 (1999)
16. J.A.C. Gallas, Appl. Phys. B **60**, S203 (1995)
17. A.R. Zeni, J.A.C. Gallas, Physica D **89**, 71 (1995)
18. A. Zeni, J.A.C. Gallas, A. Fioretti, F. Papoff, B. Zambon, E. Arimondo, Phys. Lett. A **172**, 247 (1993)
19. J.A.C. Gallas, Int. J. Bifur. Chaos **20** (2010), in press
20. J.G. Freire, R.J. Field, J.A.C. Gallas, J. Chem. Phys. **131**, 044105 (2009)
21. C. Bonatto, J.A.C. Gallas, Phys. Rev. Lett. **101**, 054101 (2008)
22. C. Bonatto, J.A.C. Gallas, Y. Ueda, Phys. Rev. E **77**, 026217 (2008)
23. C. Bonatto, J.C. Garreau, J.A.C. Gallas, Phys. Rev. Lett. **95**, 143905 (2005)
24. J.L. Borges, *El Jardín de senderos que se bifurcan (The Garden of Forking Paths)* (Editorial Sur, Buenos Aires, 1941)
25. V. Annovazzi-Lodi, A. Argyris, M. Benedetti, M. Hamacher, S. Merlo, D. Syvridis, Optics and Photonics News **19**, 36 (2008)
26. A. Uchida et al., Nat. Photon. **2**, 728 (2008)
27. I. Kanter, Y. Aviad, I. Reidler, E. Cohen, M. Rosenbluh, Nat. Photon. **4**, 58 (2009)
28. W.W. Chow, S. Wieczorek, Opt. Express **17**, 7491 (2009)
29. F.-Y. Lin, J.-M. Liu, IEEE J. Quantum Electron. **40**, 815 (2004)
30. F.-Y. Lin, J.-M. Liu, IEEE J. Quantum Electron. **40**, 991 (2004)
31. S.-C. Chan, R. Diaz, J.-M. Liu, Opt. Quantum Electron. **40**, 83 (2008)